J|A|C|S ARTICLES

Published on Web 07/09/2009

Reaction Mechanisms for the CO Oxidation on Au/CeO_2 Catalysts: Activity of Substitutional Au^{3+}/Au^{+} Cations and Deactivation of Supported Au^{+} Adatoms

Matteo Farnesi Camellone and Stefano Fabris*

Theory@Elettra Group, INFM-CNR DEMOCRITOS, c/o Sincrotrone Trieste−SS14, Km 163, 5 Basovizza, I-34012 Trieste, Italy, and SISSA Scuola Internazionale Superiore di Studi Avanzati, via Beirut 2-4, I-34014 Trieste, Italy

Received March 18, 2009; E-mail: fabris@democritos.it

Abstract: Density functional theory calculations that account for the on-site Coulomb interaction via a Hubbard term (DFT+U) reveal the mechanisms for the oxidation of CO catalyzed by isolated Au atoms as well as small clusters in Au/CeO_2 catalysts. Ceria (111) surfaces containing positively charged Au ions, either as supported Au^{+} adatoms or as substitutional Au^{3+} ions, are shown to activate molecular CO and to catalyze its oxidation to CO_2. In the case of supported single Au^{+} adatoms, the limiting rate for the CO oxidation is determined by the adsorbate spillover from the adatom to the oxide support. The reaction then proceeds with the CO oxidation via lattice oxygen and O vacancy formation. These vacancies are shown to readily attract the supported Au^{+} adatoms and to turn them into negatively charged $Au^{\delta-}$ adspecies that deactivate the catalyst, preventing further CO adsorption. Au^{3+} ions dispersed into the ceria lattice as substitutional point defects can instead sustain a full catalytic cycle consisting of three individual steps maintaining their activity along the reaction process: Au cations in $Au_xCe_{1-x}O_2$ systems promote multiple oxidations of CO without any activation energy via formation of surface O vacancies. Molecular oxygen adsorbs at these vacancies and forms O adspecies that then catalyze the oxidation of molecular CO, closing the catalytic cycle and recovering the stoichiometric $Au_xCe_{1-x}O_2$ system. The interplay between the reversible Ce^{4+}/Ce^{3+} and Au^{3+}/Au^{+} reductions underpins the high catalytic activity of dispersed Au atoms into the ceria substrate. It is shown that the positive oxidation state of the substitutional Au ions is retained along the catalytic cycle, thus preventing the deactivation of $Au_xCe_{1-x}O_2$ catalysts in operation conditions. Finally, although a single Au^{+} adatom bound to an O vacancy is shown to deactivate during CO oxidation, the calculations predict that the reactivity of gold nanoparticles nucleated at O vacancies can be recovered for cluster sizes as small as Au_2.

1. Introduction

The low-temperature oxidation of molecular CO can be efficiently catalyzed by highly dispersed Au nanoparticles supported on transition-metal oxides.[1] The activity of these catalysts is controlled by several factors, most notably the size of the metal cluster, the ability of the support to supply oxygen during the reaction, and the excess electrons at the metal/oxide interface determining the oxidation state of the gold atoms. Reducible oxides represent very active catalytic supports, and among them, ceria (CeO_2) is one of the most efficient due to its oxygen storage capacity.[2] Gold nanoclusters supported by ceria surfaces have been shown to catalyze important reactions such as low-temperature CO oxidation,[3] hydrogenation,[4] or water gas shift (WGS).[5,6]

Several experimental[7] and theoretical[8] works demonstrate the surface selectivity for CO adsorption and provide evidence that CO does not adsorb on the stoichiometric $CeO_2(111)$ surface, which represents the largest fraction of the surface exposed by conventional samples. Oxide-supported gold clusters of size smaller than 5 nm have been shown to improve the surface reactivity toward CO adsorption and oxidation.[9] The reactivity of the supported gold catalysts is controlled by several factors,

(1) (a) Grunwaldt, J. D.; Kiener, C.; Wogerbauer, C.; Baiker, A. *J. Catal.* **1999**, *181*, 223. (b) Campbell, C. T. *Science* **2004**, *306*, 234. (c) Chen, M. S.; Goodman, D. W. *Science* **2004**, *306*, 252. (d) Liu, Z.-P.; Gong, X.-Q.; Kohanoff, J.; Sanchez, C.; Hu, P. *Phys. Rev. Lett.* **2003**, *91*, 266102. (e) Mills, G.; Gordon, M. S.; Metiu, H. *J. Chem. Phys.* **2003**, *118*, 4198.

(2) *Catalysis by Ceria and Related Materials*; Trovarelli, A., Ed.; Imperial College Press: London, 2002.

(3) (a) Fierro-Gonzales, J. C.; Gates, B. C. *J. Phys. Chem. B* **2004**, *108*, 16999. (b) Fierro-Gonzales, J. C.; Gates, B. C. *Catal. Today.* **2007**, *122*, 201.

(4) Guzman, J.; Gates, B. C. *Angew. Chem., Int. Ed.* **2003**, *115*, 714.

(5) Fu, Q.; Saltsburg, H.; Flytzani-Stephanopoulos, M. *Science* **2003**, *301*, 935.

(6) Burch, R. *Phys. Chem. Chem. Phys.* **2006**, *8*, 5483.

(7) (a) Zhou, K.; Wang, X.; Sun, X.; Peng, Q.; Li, Y. *J. Catal.* **1984**, *85*, 254. (b) Aneggi, E.; Llorca, J.; Boaro, M.; Trovarelli, A. *J. Catal.* **2005**, *234*, 88.

(8) (a) Yang, Z.; Woo, T. K.; Baudin, M.; Hermansson, K. *J. Chem. Phys.* **2004**, *120*, 7741. (b) Nolan, M.; Watson, G. W. *J. Chem. Phys. B* **2006**, *110*, 16600. (c) Huang, M.; Fabris, S. *J. Phys. Chem. C* **2008**, *112*, 8643.

(9) (a) Bamwenda, G. R.; Tsubota, S.; Nakamura, T.; Haruta, M. *Catal. Lett.* **1997**, *44*, 83. (b) Valden, M.; Lai, X.; Luo, K.; Guo, Q.; Goodman, D. W. *Science* **1998**, *281*, 1647. (c) Lee, S.; Fan, C.; Wu, T.; Anderson, S. L. *J. Am. Chem. Soc.* **2004**, *126*, 5682.

10.1021/ja902109k CCC: $40.75

like the size of the gold particle size, the pretreatment conditions, and the interaction with the support. As a result, the nature of the active sites on Au/CeO_2 catalysts and the mechanisms for several reactions including CO oxidation and the WGS are still subjects of debate.

Concerning the CO adsorption and oxidation on the Au/CeO_2 system, the presence of Au^{3+}, Au^{+}, and Au^{0} species on nanocrystalline catalyst was demonstrated on the basis of IR spectroscopy.[10] This study also correlated the catalyst reactivity toward CO oxidation with the concentration of cationic Au^{3+} species, while no correlation was found with the concentration of Au^{+} and Au^{0} species. Interestingly, CO_2 was formed during the CO adsorption experiments even though the gas stream did not contain oxygen. This result indicates that the reactive oxygen taking part in the oxidation reaction was provided by the nanocrystalline CeO_2, which is well-known to present a high oxygen storage capacity and to be an efficient oxygen buffer.

In the case of the WGS reaction, Fu and co-workers[5] showed that the active species are isolated $Au^{\delta+}$ cations and that the metallic Au^{0} species do not participate into the reaction, but other recent studies[6,11−13] established that cationic gold species are not the key sites in the WGS reaction. Instead, these studies correlated the reactivity with the presence of O vacancies. In one of these studies, Rodriguez and co-workers performed different sets of experiments in order to examine the interaction of SO_2 with gold deposited on stoichiometric and partially reduced CeO_2 surfaces, as well as on AuO_x/CeO_2 systems. They showed that Au nanoparticles supported on reduced CeO_{2-x} surfaces display a considerably higher reactivity than Au nanoparticles supported on stoichiometric CeO_2 surfaces. On the basis of their results, it seems that Au nanoparticles nucleated at O vacancies of ceria should constitute the chemically active phase in reducing conditions.

Besides Au-supported catalysts, also $Ce_{(1-x)}Au_xO_{(2-\delta)}$ solid solutions have been recently proposed in the literature, although the stability of these systems is an issue of debate. Venezia and co-workers[14] used X-ray photoemission and diffraction to study gold/ceria catalysts prepared by deposition−precipitation synthesis. Their data were consistent with the presence of Au^{3+} ions in a cubic fluorite environment that was interpreted as a gold/ceria solid solution in which Au substitutes for Ce atoms. Similarly, Skoda et al.[15] investigated with photoemission spectroscopy the adsorption of CO on gold/ceria catalysts formed by sputtering. They reported partial Ce^{4+}/Ce^{3+} reductions that were interpreted by proposing the formation of a mixed Au−Ce−O surface. Further evidence for the presence of Au^{3+} ions in the bulk of a catalyst formed by sputtering was also provided more recently[16] on the basis of synchrotron-based photoelectron spectroscopy capable of sampling deep regions from the surface. It must be emphasized that, on the basis of ab initio thermodynamics,[17] the adsorption of a Au adatom on a Ce vacancy (i.e., the formation of a Au−Ce−O solid solution) would be thermodynamically favorable over the adsorption of Au adatoms on O vacancies only in extreme oxygen-rich conditions. We note that the systems interpreted to be a solid solution are formed with nonequilibrium methods, so that they might be kinetically but not thermodynamically stable.

On the theoretical side, the $Au/CeO_2(111)$ system has been investigated by several groups by using density functional theory (DFT and DFT+U) approaches. Liu et al.[18] studied the activity of small Au clusters supported on the ceria (111) surface toward the WGS reaction. Shapalov et al.[19] determined that surface O atoms are activated when a Au atom substitutes one of the Ce atoms in the $CeO_2(111)$ surface, thus proposing that these substitutional Au cations promote CO_2 desorption via the formation of O vacancies. More recently, the structural and electronic properties of gold atoms supported on ceria surfaces where characterized in detail,[17,20,21] considering a single Au adatom adsorbed on stoichiometric ceria surfaces, on reduced surfaces (substituting for a surface O vacancy), and substituting for a Ce vacancy. All these studies point to the importance of cationic Au species for CO oxidation, particularly concerning $Au^{\delta+}$ ions inserted into the CeO_2 lattice in the form of substitutional point defects.

The present computational work addresses the reaction mechanisms by which the Au/CeO_2 system catalyze the CO oxidation, as a function of the oxidation state of the Au adatoms, which is determined by the stoichiometry of the supporting oxide. We identify two different reaction mechanisms catalyzed by Au adatoms supported on the stoichiometric (111) CeO_2 surface and by Au atoms dispersed into (111) $Au_xCe_{1-x}O_{2-\delta}$ surface structures. The results show that both supported and substitutional Au atoms promote the oxidation via O vacancy formation. These vacancies can be efficiently sealed by molecular oxygen only when the Au atoms are substitutional for Ce ions, and a full catalytic cycle can be established in this case. On the contrary, the O vacancy formed during the CO oxidation attracts the supported Au^{+} adatoms during the reaction, turning them into $Au^{\delta-}$ species that prevent further CO adsorption and thus deactivate the catalyst. These species constitute aggregation sites for the nucleation of a larger cluster. We show that the reactivity of Au nanoparticles bound to an O vacancy is recovered for clusters sizes as small as Au_2.

The paper is organized as follows. The computational methodology is presented in section 2. The interaction of Au adatoms with the stoichiometric and defective $CeO_2(111)$ surfaces is studied and compared with the available literature in section 3. The adsorption of a CO molecule on these surface active sites is analyzed in section 4, where we also identify two relevant mechanisms for CO oxidation. The results are then summarized in the concluding section 5.

2. Theoretical Methods

The calculations were based on the density functional theory (DFT and DFT+U)[22] and employed the exchange and correlation energy functional expressed in the Perdew−Burke−Ernzerhof

(10) Guzman, J.; Carrettin, S.; Corma, A. *J. Am. Chem. Soc.* **2005**, *127*, 3286.
(11) Rodriguez, J. A.; Pérez, M.; Evans, J.; Liu, G.; Hrbek, J. *J. Chem. Phys.* **2005**, *122*, 241101.
(12) Tabakova, T. J.; Boccuzzi, F.; Manzoli, M.; Andreeva, D. *Appl. Catal* **2003**, *252*, 385.
(13) Wang, X.; Rodriguez, J. A.; Hanson, J. C.; Pérez, M.; Evans, J. *J. Chem. Phys.* **2005**, *123*, 211101.
(14) Venezia, A. M.; Giuseppe, P.; Longo, A.; Di Carlo, G.; Casaletto, M. P.; Liotta, F. L.; Deganello, G. *J. Phys. Chem. B* **2005**, *109*, 2821.
(15) Skoda, M.; Cabala, M.; Matolinova, I.; Prince, K. C.; Skala, T.; Sutara, F.; Veltruska, K.; Matolin, V. *J. Chem. Phys.* **2009**, *130*, 034703.
(16) Matolin, V.; Cabala, M.; Matolinova, I.; Skoda, M.; Libra, J.; Vaclavu, M.; Prince, K. C.; Skala, T.; Yoshikawa, H.; Yamashita, Y.; Ueda, S.; Kobayashi, K. *J. Phys. D: Appl. Phys.* **2009**, *42*, 115301.
(17) (a) Zhang, C; Michaelides, A.; King, D. A.; Jenkis, S. J. *J. Chem. Phys.* **2008**, *129*, 194708. (b) Zhang, C.; Michaelides, A.; King, D. A.; Jenkis, S. J. *J. Phys. Chem. C* **2009**, *113*, 6411.
(18) Liu, Z. P.; Jenkins, S. J.; King, D. A. *Phys. Rev. Lett.* **2005**, *94*, 196102.
(19) Shapalov, V.; Metiu, H. *J. Catal.* **2007**, *245*, 205.
(20) Nolan, M.; Verdugo, V. S.; Metiu, H. *Surf. Sci.* **2008**, *602*, 2734.
(21) Chen, Y.; Lee, M.-H.; Wang, H. *Surf. Sci.* **2008**, *602*, 1736.

(PBE) generalized gradient approximation (GGA).[23] The spin-polarized Kohn−Sham equations were solved in the plane-wave pseudopotential framework, with the wave function basis set and the Fourier representation of the charge density being limited by kinetic cutoffs of 30 and 300 Ry, respectively. The ions were described by ultrasoft pseudopotentials[24] obtained for the following atomic configurations: Au $[Xe]4f^{14}|5d^{9.5}6s^{1}6p^{0.5}$, Ce $[Kr]4d^{10}|5s^{2}5p^{6}4f^{1}5d^{1}6s^{2}$, and O $[He]|2s^{2}2p^{4}$. The calculations have been performed with the Quantum-ESPRESSO computer package.[25]

It is now well-established that the addition to the standard density functional of a Hubbard U term acting on the Ce 4f orbitals allows for an accurate description of the electronic structure of both oxidized and reduced ceria structures.[26−30] In the present DFT+U work we have used the implementation of Cococcioni and de Gironcoli[31] and a value of $U = 4.5$ eV, in line with previous analysis.[26,27] The occupations of the f states have been calculated by means of a projector defined in terms of atomic-like wave functions. The dependency of the calculated results on the value of the parameter U will be discussed in the text.

The study of gold adatoms supported by the stoichiometric ceria surface and by the reduced surface (gold atom into an oxygen vacancy) has been carried out with orthorhombic (2×2) nine-layer supercell slabs (12 CeO_2 units per supercell) separated by more than 15 Å of vacuum. Brillouin zone integration has been performed on a ($2 \times 2 \times 1$) Monkhorst−Pack grid.[32] The simulation of a gold atom substituting for a surface Ce atom requires larger supercells and has been done with hexagonal (3×3) nine-layer supercell slabs (27 CeO_2 units per supercell) separated by more than 15 Å of vacuum. In this case, the Brillouin zone integration has been performed on the Γ point only. The lowermost three atomic layers of the supercells have been constrained to the equilibrium positions, while all other atoms were allowed to relax according to the calculated Hellman−Feynman forces[33] until the maximum force was less than 0.02 eV/ Å. The reaction mechanism for CO oxidation has been studied by means of the climbing image nudged elastic band (CI-NEB) method[34] that was used to identify the minimum energy paths on the potential energy surface. These calculations have been performed in the supercells described above including up to 20 replica images.

Adsorption energies have been calculated using the formula $E_{ads} = E_{tot} - (E_{sub} - E_X)$, where E_{tot} is the total energy of the combined system (namely the adsorbate X bound to the substrate), E_{sub} is the energy of the substrate alone, and E_X is the total energy of the adsorbate in the gas phase. With a similar spirit, the bonding charge density has been evaluated using the expression: $\Delta\rho(\mathbf{r}) = \rho_{X/CeO_2(111)}(\mathbf{r}) - \rho_{CeO_2(111)}(\mathbf{r}) - \rho_X(\mathbf{r})$, where $\rho_{X/CeO_2(111)}(\mathbf{r})$, $\rho_{CeO_2(111)}(\mathbf{r})$, and $\rho_X(\mathbf{r})$ are the charge density of the whole system, the isolated substrate, and the adsorbate, respectively.

Table 1. Adsorption Energies (E_a) of a Au Adatom on the Bridge and Top Sites of the Stoichiometric CeO_2(111) Surface As Well As on an O and Ce Vacancy (Au@ V_O and Au@V_{Ce})[a]

		ref 21				
		BLYP	PBE+U	PBE+U	ref 17a: PBE+U	this work: PBE+U
Au@O(bridge)	E_a	−0.63	−0.79	−0.88	−1.17	−1.18
Au@O(top)	E_a				−0.96	−1.04
Au@V_O	E_a	−2.72	−3.20	−2.58	−2.75	−2.29
	$E_f^{CeO_2}$ (V_O)	3.17	3.56	2.61	2.67	2.15
	$E_a + E_f$ (V_O)	0.45	0.36	0.02	−0.07	−0.14
Au@V_{Ce}	E_a	−5.15	−5.64	−5.65	−5.94	−5.68
	E_f^{Au/CeO_2} (I V_O)	0.19	−0.16	−0.01		0.32
	E_f^{Au/CeO_2} (II V_O)	1.40	1.63	0.86		1.61

[a] In the latter cases, we also indicate the energy for creating an O vacancy (E_f) on the stoichiometric [E_f^{CeO2} (V_O)] surface and for creating a first and a second O vacancy in the Au@V_{Ce} system [$E_f^{Au/CeO2}$ (I V_O) and $E_f^{Au/CeO2}$ (II V_O), respectively].

3. Bonding of Au Adatoms to the CeO_2(111) Surface

3.1. Au Adatoms on the Stoichiometric Surface. The calculations predict the existence of two stable adsorption sites (bridge and top) of a Au adatom on the stoichiometric (111) surface of ceria, differing by 0.14 eV in energy. We anticipate that this small energy difference between the two adsorption configurations plays an important role in the mechanism for CO oxidation. The Au adatom initially located on either of the two symmetry-inequivalent hollow sites of the CeO_2(111) surface relaxes into the lowest-energy bridging configuration. In all cases, the interaction between the Au atom and the CeO_2 surface involves a charge transfer from the adsorbate to the substrate, yielding the reduction of a Ce ion.

The most stable adsorption configuration for a Au adatom is the bridge site between two surface O atoms. The calculated adsorption energy and the Au−O bond length are −1.18 eV and 2.18 Å, respectively, in good agreement with recent works[17a] reporting −1.17 eV and 2.19 Å (Table 1). The bonding charge analysis (Figure 1A,B) reveals that ∼0.17 e are transferred from the metal to the oxide surface, leading to the formation of a positively charged $Au^{\delta+}$ ion, which on the basis of charge population analysis we interpret as Au^+ (see Supporting Information). This magnitude of charge transfer, corresponding to the shaded area in Figure 1a, is obtained by integrating the bonding charge on planes parallel to the surface from the middle of the vacuum region to the middle of the Au−O bond length. The excess charge in the substrate (Figure 1b) is mostly localized around the surface O atoms bound to Au and on one Ce^{4+} ion, which reduces to Ce^{3+}. This is corroborated by the calculated density of electronic states (DOS, Figure 1c) that displays two new features in the band gap, labeled "A" and "B". The projected DOS analysis (PDOS, Figure 1c) reveals that the gap state A closest to the valence band is related to the Au−O bonding, since it results from the overlap between the Au(d) states and the O(p) states of the surface O atoms nearest neighbor to the adsorbate (labeled as O* in Figure 1 and hereafter). A more detailed analysis reveals that the Au−O* bond results almost exclusively from the overlap of the Au(d_{zx}) and Au(d_{zy}) with the O*(p_x) and O*(p_y) states. In addition, the overlap between the same orbitals gives rise to a new state at the bottom of the valence band (C). The gap state B closest to

(22) Hohenberg, P.; Kohn, W. *Phys. Rev.* **1964**, *136*, B864. Kohn, W.; Sham, L. *J. Phys. Rev.* **1965**, *140*, A1133.
(23) Perdew, J. P.; Burke, K.; Ernzerhof, M. *Phys. Rev. Lett.* **1996**, *77*, 3865.
(24) Vanderbilt, D. *Phys. Rev. B.* **1990**, *41*, R7892.
(25) Quantum-ESPRESSO is a community project for high-quality quantum-simulation software, based on density-functional theory, and coordinated by Paolo Giannozzi. See http://www.quantum-espresso.org and http://www.pwscf.org
(26) Fabris, S.; de Gironcoli, S.; Baroni, S.; Vicario, G.; Balducci, G. *Phys. Rev. B* **2005**, *71*, 041102.
(27) Fabris, S.; Vicario, G.; Balducci, G.; de Gironcoli, S.; Baroni, S. *J. Phys. Chem. B* **2005**, *109*, 22860.
(28) Nolan, M; Parker, S. P.; Watson, G. W. *Surf. Sci.* **2005**, *595*, 223.
(29) Loschen, C.; Carrasco, J.; Neyman, K. M.; Illas, F. *Phys. Rev. B* **2006**, *75*, 035115.
(30) Da Silva, J. L. F.; Ganduglia-Pirovano, M. V.; Sauer, J.; Bayer, V.; Kresse, G. *Phys. Rev. B* **2006**, *75*, 045121.
(31) Cococcioni, M.; de Gironcoli, S. *Phys. Rev. B* **2005**, *71*, 035105.
(32) Monkhorst, H. J.; Pack, J. D. *Phys. Rev. B* **1976**, *13*, 5188.
(33) Feynman, R. P. *Phys. Rev.* **1939**, *56*, 340.
(34) Jónsson, H.; Mills, G.; Jacobsen, K. W. *Classical and Quantum Dynamics in Condensed Phase Simulations*; World Scientific: Singapore, 1998; Chapter 16, p 385.

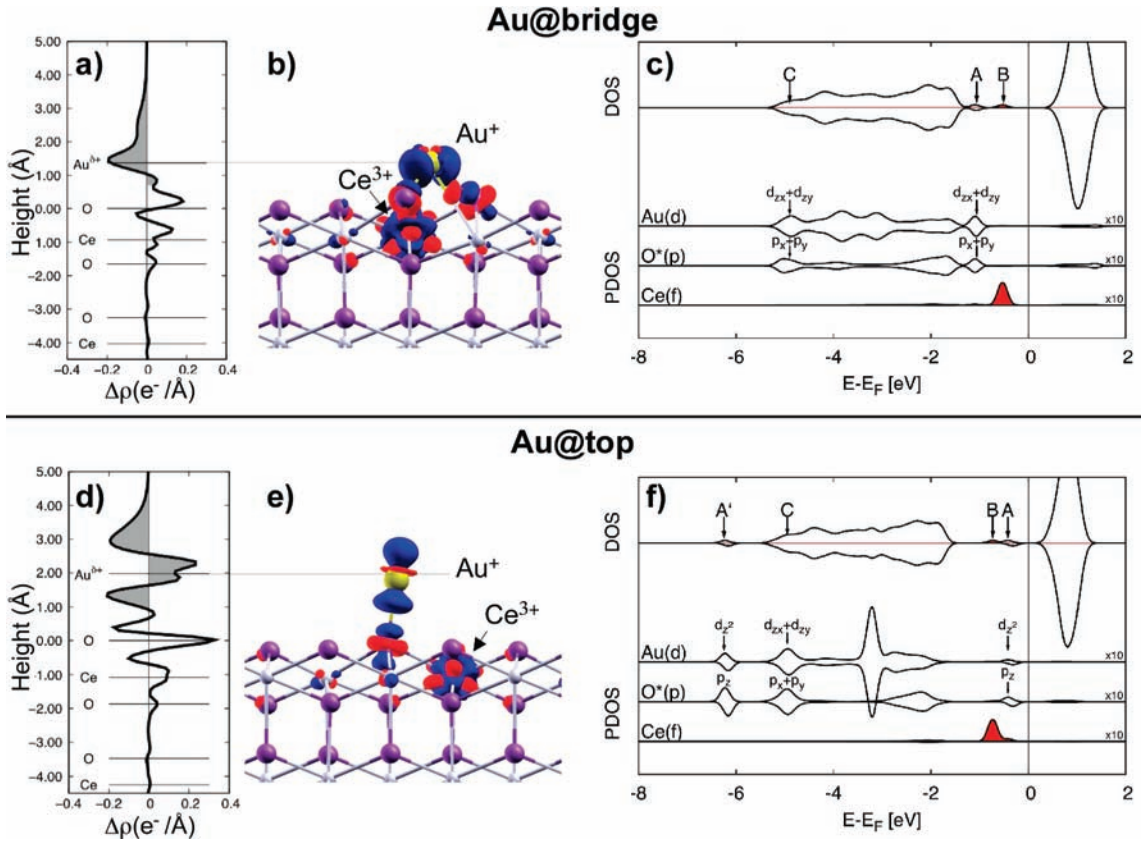

Figure 1. Calculated bonding charge ($\Delta\rho$) and density of electronic states (DOS) for a Au adatom supported by the stoichiometric (111) surface in the bridge (panels a−c) and top (panels d−f) configurations. Left panels (a and d) represent the bonding charge integrated in planes perpendicular to the surface and plotted as a function of the height from the surface. Central panels (b and e) display the bonding charge plotted at the value of 0.06 electrons/Å^3. Electron accumulation and depletion are represented by red and blue areas, respectively. Right panels (c and f) display the total DOS and atom-resolved projected DOS (PDOS) analysis. Energies are referred to the Fermi level, which is marked by a vertical solid line.

the Fermi level results instead from the charge transferred to the substrate and localized on the Ce(f) state, leading to the $Ce^{4+} \rightarrow Ce^{3+}$ reduction. The total spin polarization of this ground state is 1.00 μ_B and is determined by the unpaired excess electron localized on the Ce^{3+} ion.

The lowest energy position of the one-electron defect (Ce^{3+} ion) is third neighbor to the adsorbate, at 4.76 Å in the surface direction along the Au−O bond. This is consistent with the result of Zhang and co-workers,[17a] but, in contrast to that study, we were also able to stabilize a self-consistent solution 0.07 eV higher in energy in which the excess electron localizes on the Ce site second neighbor to the Au adatom (at 3.34 Å). This result is in line with the recent works in the context of electron localization near O vacancies on the (111) surface,[35] where the energy difference between the two configurations in which the Ce^{3+} ion was located nearest neighbor or next nearest neighbor to the vacancy is 0.1 eV/Ce ion in favor of the latter configuration.

The calculated adsorption energy for the metastable top adsorption site is −1.04 eV, and the resulting Au−O bond length is 2.00 Å, slightly shorter than that of the most stable bridge configuration. Despite the very small difference in adsorption energy with the bridge site, the Au−O interaction involves different orbitals. The integrated charge difference profile along a direction perpendicular to the surface (Figure 1d) presents marked differences with the one for the bridge configuration (Figure 1a), the most relevant being in the region between the Au and the O* atoms. Here, adsorption on the bridge (top) site induces charge accumulation (depletion). Overall, also in this metastable configuration there is a net charge transfer of ∼0.14 e from the metal adatom to the surface (shaded area in Figure 1d), leading to a positively charged $Au^{\delta+}$ adatom and to the reduction of one Ce ion. This charge redistributes in the substrate mostly by localizing on one of the Ce sites nearest neighbor to the adatom and partly on the O* atom involved in the Au−O bond (Figure 1e). Moreover, also in this case there are two new filled electronic states in the band gap (A and B, see DOS displayed in Figure 1f), but they have reversed relative energy ordering with respect to the corresponding ones in the lowest energy bridge adsorption site. The gap state closer to the valence band (B) is now the one localized on the Ce(f) orbital (see PDOS in Figure 1f), whose energy, controlled in the calculations mostly by the value of the U parameter, is 0.2 eV lower the corresponding one for the bridge site. The gap state closer to the Fermi energy (A) results instead from the Au−O* interaction, which in this case clearly shows a smaller overlap between the Au(d) and the O*(p) states (PDOS in Figure 1f). As a result, its energy is shifted at higher values from −1.05 eV (bridge site) to −0.42 eV (top site) with respect to the Fermi level. Quite consistently, the Au−O* bonding orthogonal to the surface involves the Au(d_{z^2}) and the O(p_z) states, whose overlap also originates an additional electronic state (A′ in Figure 2) 6.27 eV below the bottom of the valence band.

(35) Ganduglia-Pirovano, M. V.; Da Silva, J. L.; Sauer, J *Phys. Rev. Lett.* **2009**, *102*, 026101.

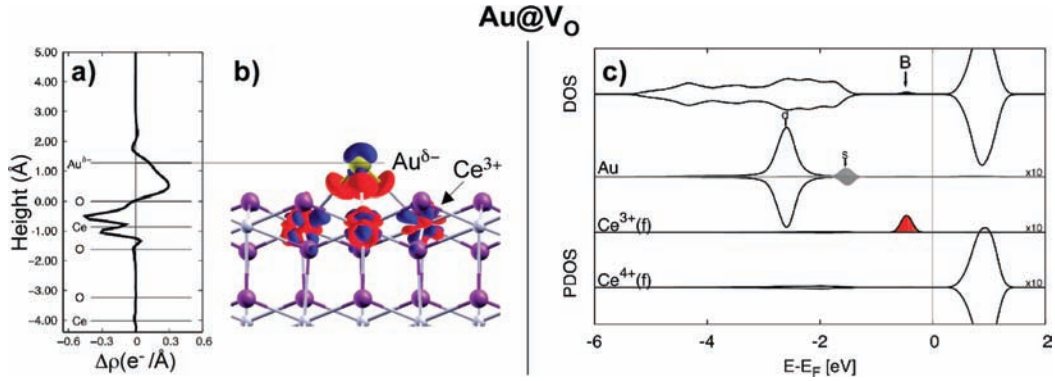

Figure 2. Calculated bonding charge ($\Delta\rho$) and density of electronic states (DOS) for a Au adatom adsorbed on a surface O vacancy. (a) Bonding charge integrated in planes perpendicular to the surface and plotted as a function of the height from the surface. (b) Bonding charge displayed at the value of 0.06 electrons/Å^3. Electron accumulation and depletion are represented by red and blue areas, respectively. (c) Total DOS and atom-resolved projected DOS (PDOS) analysis. Energies are referred to the Fermi level, which is marked by a vertical solid line.

3.2. Au Adatoms at Oxygen Vacancies of Reduced Surfaces. Surface oxygen vacancies result in very stable anchoring sites for a Au adatom, which binds at 1.3 Å above the O vacancy site with two Ce* nearest neighbors at 3.14 Å (Au−Ce^{4+}) and one at 3.20 Å (Au−Ce^{3+}). This bond length asymmetry is due to the response of the adsorbate to the different electron occupation of the f states of the nearest-neighbor Ce atoms. In the case of an isolated O vacancy, the charge neutrality is maintained by the presence of two Ce^{3+} ions. The binding of a Au atom on an O vacancy site entails a strong charge rearrangement at the Au/oxide contact. The bonding charge distribution for this final state (Figure 2a) shows that the charge transfer occurs now from the reduced oxide surface (from one of the two Ce^{3+} ion that oxidizes to Ce^{4+}) to the supported metal atom, thus leaving a reduced surface with just one Ce^{3+} ion. This results into a negatively charged Au$^{δ-}$ adatom and leads to the formation of directional Au−Ce* covalent bonds (red areas in Figure 2b) similar to those predicted for Au clusters supported by reduced TiO_2.[36]

Only one filled electron state is present in the band gap (labeled "B" in the DOS of Figure 2c) that results from one electron being localized on the f state of the Ce^{3+} ion nearest neighbor to the Au adsorbate. The PDOS for the Au adatom displays two sharp peaks that can be associated with the s states, which are at the top of the valence band (shaded gray area in Figure 2c), and to the d states, which are 1.06 eV lower in energy. This allow us to conclude that the charge transferred from one of the Ce^{3+} ions of the isolated surface vacancy to the Au adatom adsorbed on the vacancy populates the Au(s) states, whose spatial distribution is clearly displayed by the red hemicycles in Figure 2 centered between the Au−Ce* bonds. This electronic structure, together with the charge transfer discussed above, suggests that the bonding of Au adatoms to O vacancies of the reduced (111) CeO_2 surface has a mixed ionic character with a partial covalent contribution.

The GGA+U calculated adsorption energy of a Au adatom on an O vacancy is −2.29 eV (GGA+U, GGA value is −3.22 eV), much larger than the binding to the bridge site of the stoichiometric (111) surface. The higher stability of Au adatoms into the O vacancy with respect to the stoichiometric surface is at the basis of the deactivation mechanism during CO oxidation that will be discussed in section 4. The calculated adsorption energy is smaller than that reported by previous results obtained with the GGA-PBE functional that however show a considerable degree of variation, being −3.20,[21] −2.58,[21] and −2.75 eV,[17a] (Table 1). We remark that the DFT+U energy differences are strongly dependent on the value of the parameter U and on the choice of projector functions used to calculate the occupancies when the initial and final states differ in the occupation of the Ce(f) states involved in the Hubbard term of the Hamiltonian.[26−30]

It is interesting to compare the energy of Au adsorption to an O vacancy (E_{ads}) with the energy required to form the surface vacancy (E_v), which is 2.15 eV for the present orthorhombic (2 × 2) supercell, calculated with respect to molecular O_2, whose energy was corrected for the overbinding of the PBE functional (Table 1). The term (E_{ads}+ E_v) measures the heat released by the overall process consisting of vacancy formation and Au adsorption from the gas phase into the vacancy. Our result (reported in Table 1 and compared with the literature) for this energy difference is −0.14 eV, in good agreement with the value of −0.07 eV of Zhang and co-workers,[17a] suggesting that the overall process is energetically favorable, although we note that other calculations report positive values ranging between 0.02 and 0.36 eV.[21]

3.3. Au Atoms Dispersed into the CeO_2 Lattice. $Ce_{(1-x)}Au_xO_{1-δ}$ solid solutions in which Au atoms are incorporated into the ceria lattice as substitutional point defects have been proposed in the literature on the basis of several photoemission experiments;[14−16] however, we are not aware of any direct crystallographic evidence for the stability of these alloys. We have studied this case by substituting one Ce atom of the second atomic layer of the (111) surface with a Au atom. This problem requires larger computational supercells than those used to address the adsorption of adatoms on the stoichiometric CeO_2 surface. The hexagonal (3 × 3) supercell is employed in this part of the study. The presence of the Au substitutional point defect induces a strong rearrangement of the neighboring atoms, leading to the formation of a characteristic distorted square-planar AuO_4 unit (Figure 3a). In this configuration, the gold atom is coordinated by two O atoms of the first layer (at 2.14 Å) and by two of the second layer (at 2.14 Å). In addition, there are two apical O atoms located above and below the AuO_4 unit, with Au−O bond lengths of 2.38 and 2.42 Å, respectively. In the absence of O vacancies, the dispersion of Au into the ceria lattice does not yield a change in the occupation of the Ce(f) states; hence, all Ce ions maintain their formal oxidation state of 4+.

(36) (a) Matthey, D.; Wang, J. G.; Wendt, S.; Matthiesen, J.; Schaub, R.; Laegsgaard, E.; Hammer, B.; Besenbacher, F. *Science* **2007**, *315*, 1692. (b) Wang, J. G.; Hammer, B. *Phys. Rev. Lett.* **2006**, *97*, 136107.

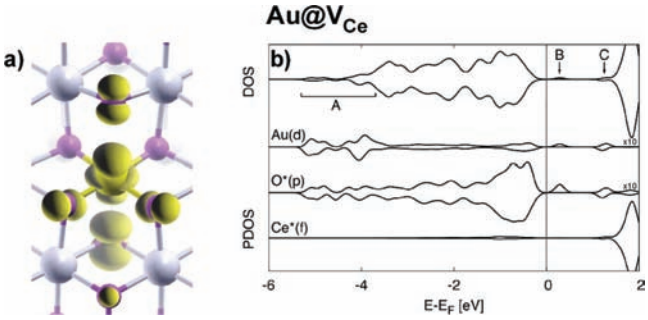

Figure 3. (a) Spin density for a Au atom substituting for a Ce site plotted at the value of 0.03 electrons/Å^3, and (b) total DOS and atom-resolved projected DOS (PDOS) analysis. Energies are referred to the Fermi level, which is marked by a vertical solid line.

This is demonstrated by the atom-resolved PDOS analysis (Figure 3b), where all the Ce* ions nearest neighbor to the substitutional Au defect (at a distance of 3.83 Å) display unoccupied f states. The features resulting from the Au−O* bonding are mostly located in the energy range labeled "A" at the bottom of the valence band. In addition, there are two unoccupied gap states (B and C in Figure 3c); the former results from the overlap of the Au($d_{x^2-y^2}$) and Au(d_{zy}) with the O*(p) states, and the latter from the overlap of the Au(d_{xy}) with the O*(p) states. Both of them control the reversible change of oxidation state $Au^{3+}-Au^{+}$ that assists the oxidation of CO, as described in the following. The system has a spin polarization of 1 μ_B that is spatially localized on the Au (22%) an on the neighboring O* atoms (12% on each the three surface O* atoms and 43% on the O* atom of the third layer), as displayed in Figure 3a.

The calculated adsorption energy for a Au atom into a preformed Ce vacancy is −5.68 eV, in good agreement with the literature reporting values between −5.15 and −5.94 eV (Table 1). We remark that the formation of a Au point defect substitutional for a Ce ion does not reduce the ceria surface; hence, the calculated GGA+U adsorption energy is independent of the value of *U* and is equal to the GGA result. This large value of the adsorption energy, suggesting a strong preference for Au atoms to enter into the ceria lattice, has however to be compensated by the energy for creating the Ce vacancy, 4.85 eV.[17a] As discussed by Zhang and co-workers,[17a] by introducing this offset, the adsorption energy of Au on the Ce vacancy is still more negative (−1.02 eV) than the one calculated for the adsorpion on an O vacancy (−0.14 eV). The same authors[17b] have recently coupled these data with the ab initio thermodynamic approach to consider the effect of the environment, showing that the adsorption of Au on the Ce vacancy becomes favorable over the O vacancy site only in extreme O-rich reaction conditions.

4. CO Oxidation on Supported and Dispersed Au Atoms

In the following, we study the reactivity of single gold atoms as a function of their oxidation state, which is determined by the stoichiometry of the supporting oxide. To this end, we consider the interaction of a CO molecule with the systems characterized in section 3, namely a gold atom on the stoichiometric and inside an oxygen vacancy of the reduced (111) surface (section 4.1), as well as occupying a Ce site of the (111) surface, i.e. dispersed as a substitutional point defect (section 4.2).

4.1. Surface-Supported Au Adatoms and Clusters.

4.1.1. CO Molecular Adsorption. The adsorption of a CO molecule on a Au adatom in the lowest-energy bridge surface site is strongly exothermic, releasing −2.48 eV (GGA+U, while −1.94 at the GGA level). Upon adsorption of the CO molecule, the adatom spontaneously diffuses from the bridge site to the top site, leading to the configuration shown in Figure 4, in which the Au adatom is aligned with the CO molecule along the direction normal to the surface. The C−O bond length of the adsorbed molecule is 1.15 Å, essentially unaffected with respect to the calculated gas-phase value (1.14 Å); the distance between the C atom and the Au adatom is 1.89 Å, while the Au adatom is 1.96 Å above a surface O* atom.

The change of adsorption site of the Au adatom from bridge to top is related to the small energy difference separating the two adsorption configurations and to the specific overlap between the Au(d) and O*(p_z) states, whose direction is compatible with the vertical adsorption configuration. Indeed, the bonding charge analysis (displayed in Figure 4 and calculated with respect to the charge density of a Au adatom in the top site) clearly shows the charge transfer from the Au^+ adatom to the p_z orbitals of both the O* and C atoms at the Au/oxide and Au/CO contacts, respectively. This charge can be transferred more easily from the Au top configuration, whose highest occupied state is indeed due to the O(p_z) states (see state A in the DOS of Figure 4) overlapping with the Au(d_{z^2}) rather than from the Au bridge configuration, in which the highest occupied state is a surface Ce(f) state (state B in Figure 1). At the Au/CeO_2 contact, the charge redistribution does not reduces further the oxide support, since only one Ce^{3+} ion is present before and after adsorption (state B in Figure 4c), but it involves only the Au(d)−O*(p) overlap (states A and C in Figure 4). On the molecular side, charge is also transferred to the C(p_z) states (D in Figure 4b). This is confirmed by the bonding charge analysis displayed in Figure 4, in which the regions of charge depletion (blue areas) are consistent with the Au(d_{zx} and d_{zy}) states, while both the O*(p_z) and C(p_z) orbitals are involved in charge accumulation (red areas).

4.1.2. CO Oxidation and Catalyst Deactivation. Several theoretical studies have addressed the oxidation of CO catalyzed by gold atoms supported by different oxides.[37] In most of them, the oxidation has been modeled in the presence of oxygen adspecies yielding to the formation of surface CO−O intermediate complexes that leads to CO oxidation and CO_2 desorption. In this section, we propose a different oxidation mechanism that does not imply the presence of oxygen adspecies and that takes advantage of the specific oxygen buffering capacity of ceria.

The calculated reaction path for this mechanism is illustrated in Figure 5 and involves three steps: the spillover of the CO molecule, the actual oxidation via a lattice oxygen atom leading to CO_2 desorption, and the diffusion of the Au adatom into the newly formed O vacancy. We note that the oxidation process does not modify the degree of reduction of the oxide support, which entails the presence of one singe Ce^{3+} ion from the initial to the final state. As a result, the calculated energy barriers are weakly depending on the specific value of the parameter *U* (in the following, both GGA and GGA+U results will be indicated).

The rate-limiting step of the overall reaction is the molecular spillover, requiring an activation energy of 0.78/0.86 eV (GGA/

(37) (a) Molina, M. L.; Hammer, B. *Phys. Rev. Lett.* **2003**, *90*, 206102. (b) Remediakis, I. N.; Lopez, N.; Nørskov, J. K. *Angew. Chem., Int. Ed.* **2005**, *44*, 1824. (c) Hernandez, N. C.; Sanz, J. F.; Rodriguez, J. A. *J. Am. Chem. Soc.* **2006**, *128*, 15600.

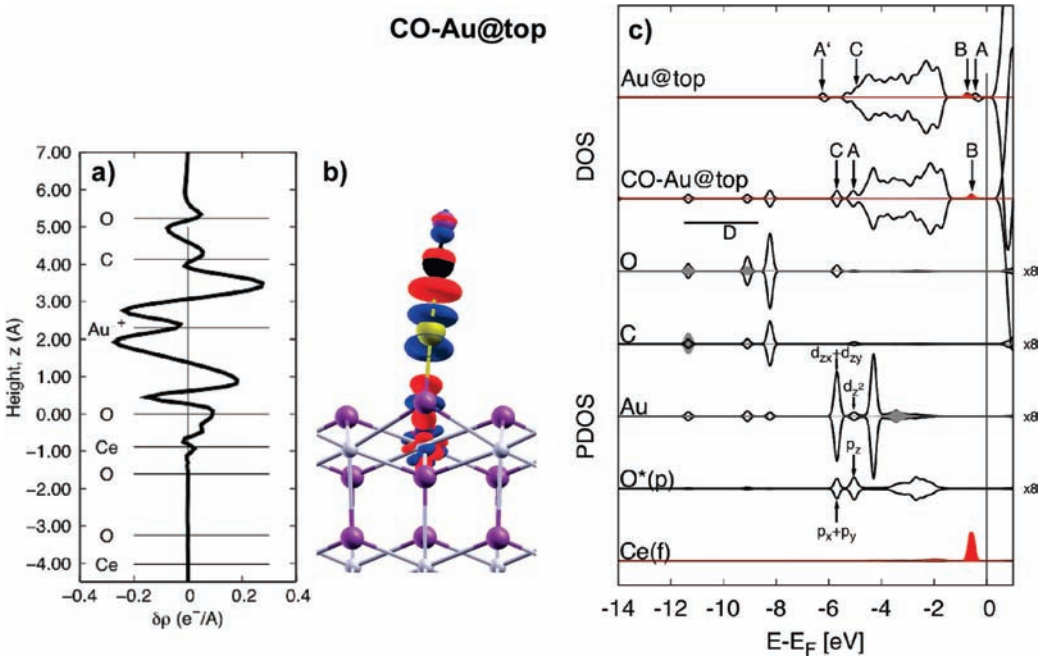

Figure 4. Calculated bonding charge ($\Delta\rho$) and density of electronic states (DOS) for a CO molecule adsorbed on a supported Au adatom. (a) Bonding charge integrated in planes perpendicular to the surface and plotted as a function of the height from the surface. (b) Bonding charge displayed at the value of 0.06 electrons/Å^3. Electron accumulation and depletion are represented by red and blue areas, respectively. (c) Total DOS and atom-resolved projected DOS (PDOS) analysis. Energies are referred to the Fermi level, which is marked by a vertical solid line.

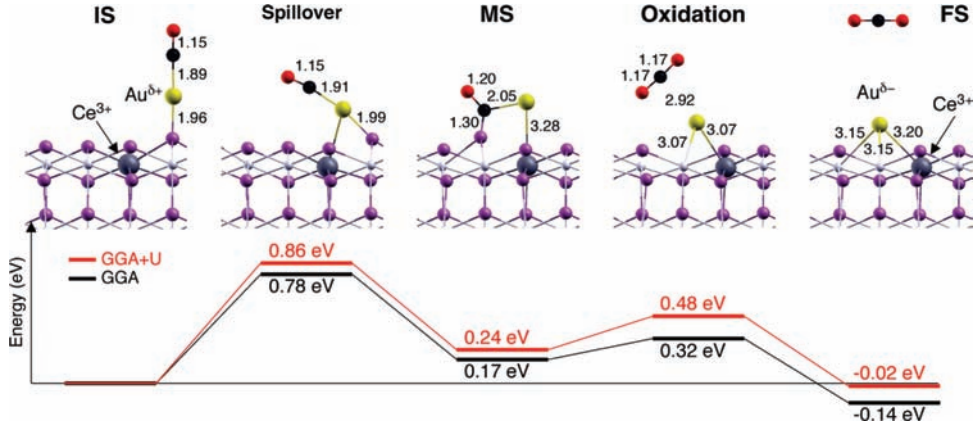

Figure 5. Calculated reaction path and corresponding energetics for the oxidation of molecular CO catalyzed by a supported Au^+ adatom. The energy differences are referred to the initial state (IS), and the relevant bond lengths are indicated in the top panels and are expressed in angstroms.

GGA+U) and leading to a metastable Au−COO* configuration (MS in Figure 5) in which the CO molecule bridges between the Au^+ and the closest surface O atom. During the spillover, the Au adatom moves from the top site back to a bridge position and both the Au−C and the C−O bond lengths elongate, with respect to the initial state, to 2.05 and 1.21 Å, while the new C−O* bond length is 1.31 Å.

The calculated activation energy for the following oxidation step, leading to CO_2 desorption and O vacancy formation, is just 0.15/0.24 eV (GGA/GGA+U). During the oxidation, the single Au^+ adatom close to the O vacancy is readily attracted into the vacancy region, leading to the local structure described in section 3.2. The final state of the reaction consists therefore of a negatively charged $Au^{\delta-}$ adatom on top of an oxygen vacancy.

The resulting $Au^{\delta-}$ adatom is highly stable (calculated GGA+U binding energy of −2.29 eV) and, most importantly, does not allow for the adsorption of other CO molecules. As a result, the oxidation of a CO molecule is effectively catalyzed by a single Au adatom, but during the reaction the catalyst deactivates since a CO molecule initially located end-on at 2.0 Å over this $Au^{\delta-}$ species does not bind and relaxes readily back in the gas phase. Molecular oxygen could in principle regenerate the catalyst by sealing the vacancy and recovering the active Au^+ adspecies. It turns out that the $Au^{\delta-}$ is inert also toward O_2 adsorption, a necessary intermediate for the catalyst regeneration.

These results suggest the existence of a critical cluster size, for which the spillover step could still be active, but the Au−Au cohesion of the cluster would constrain the diffusion of the interfacial Au ions into the O vacancy, hence hindering the deactivation and preserving the reactivity of the interfacial Au^+ atoms, as suggested for Au/TiO_2 systems.[36] This observation is in agreement with recent experimental data[38] showing that the binding of molecular CO to Au/CeO_2 catalysts is determined

(38) Weststrate, C. J.; Westerstrom, R.; Lundgren, E.; Mikkelsen, A.; Andersen, J. N. *J. Phys. Chem.* **2008**, *113*, 724.

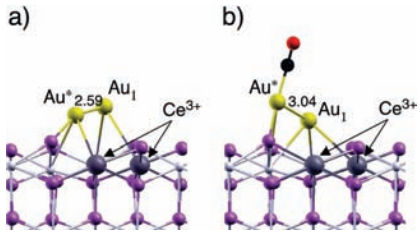

Figure 6. Relaxed geometry of a Au_2 cluster bound to an O vacancy of the $CeO_2(111)$ surface (a) and modifications induced by molecular adsorption of CO (b). The Au−Au bond lengths are expressed in angstroms.

by the size of the supported Au nanoparticles. Small Au nanoparticles supported by reduced ceria are shown to bind molecular CO more weakly and in smaller amounts than similarly sized nanoparticles supported by oxidized ceria. Both effects are most pronounced for small Au particles and disappear when the Au average particle size increases.

4.1.3. Cluster Nucleation at O Vacancies and Activity of Supported Au_2. Since thermodynamic arguments predict the O vacancies to be the preferred sites for the adsorption of Au adatoms, it is expected that, similarly to other oxide supports like TiO_2,[36,39] also in the case of ceria O vacancies will play a major role in the nucleation of supported Au clusters. Many experimental studies suggest that Au can be supported on ceria in the form of small clusters that aggregate nearby the initial $Au^{\delta-}/CeO_{(2-x)}$ system considered above.[11−13] We have shown that these catalytic sites (a single Au adatom bound to an O vacancy) prevent the formation of stable intermediates for the CO oxidation reaction, i.e., CO adsorbates. In this context, it is interesting to investigate which is the minimum cluster size Au_n that nucleates at the O vacancies and that allow for the binding of molecular CO.

To this end, we consider here the case of a Au_2 dimer adsorbed on an O vacancy, whose calculated structure is shown in Figure 6a. A second Au atom (denoted as Au*) binds with −1.98 eV to the $Au_1/CeO_{(2-x)}$ system, and induces the reduction of a further Ce ion, thus leading to a Au_2 dimer above an O vacancy with two Ce^{3+} ions. The dimer is tilted with respect to the surface, the Au* atom being closer to the surface than the Au_1 atom originally above the O vacancy. The characteristic bond lengths are included in Figure 6. What we want to emphasize here is the finding that a cluster as small as Au_2 allows for the formation of stable CO adsorbates.

A CO molecule originally positioned above the Au_2 cluster at 2.61 and 2.81 Å from the Au_1 and Au* atoms, respectively, is predicted to reach the binding configuration shown in Figure 6b. In contrast to the case of the $Au_1/CeO_{(2-x)}$ system, the molecule binds to the Au_2 cluster, with a calculated adsorption energy of −1.60 eV. This value is smaller than that one obtained for the adsorption of CO on a Au adatom supported by the stoichiometric surface (−2.48 eV). The CO molecule binds to the Au* atom, which is the most distant from the O vacancy and induces a considerable reorganization of the supported cluster: The Au−Au distance elongates from 2.59 Å (Figure 6a) to 3.04 Å (Figure 6b); The Au* atom, originally closer to the oxide surface, relaxes outward by 0.60 Å, while the Au_1 atom closer to the vacancy relaxes inward toward the vacancy by 0.47 Å, thus reverting the tilting of the Au_2 dimer.

(39) Wahlstrom, E.; Lopez, N.; Schaub, R.; Thostrup, P.; Rønnau, A.; Africh, C.; Lægsgaard, E.; Nørskov, J. K.; Besenbacher, F. *Phys. Rev. Lett.* **2003**, *90*, 026101.

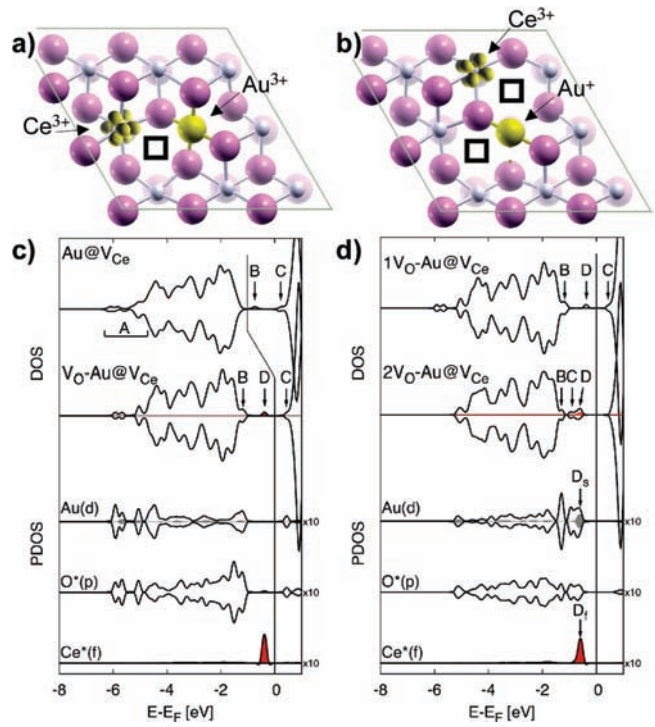

Figure 7. Top view of the surface structures and spin densities resulting from the first [(a) V_O−Au@V_{Ce}] and second [(b) 2 V_O−Au@V_{Ce}] CO oxidations catalyzed by a Au atom substituting for a Ce ion in the (111) surface, together with the corresponding total DOS and PDOS analysis (c and d). Oxygen vacancies are represented by white squares. The total DOS of the initial state in both reactions (Au@V_{Ce} and V_O−Au@V_{Ce}) are also included for reference.

A full description of the atomistic and electronic structure of Au clusters supported on ceria will be the subject of a separate report. These results for the simplest of the Au clusters provides evidence that, although a single adatom supported on the stoichiometric surface can be deactivated during CO oxidation, the resulting inactive $Au^{\delta-}$ species favor the aggregation of further Au adatoms. In this way, the activity toward CO oxidation is recovered for cluster sizes as small as Au_2.

4.2. CO Oxidation by Au Adatoms Dispersed into the $CeO_2(111)$ Surface.

4.2.1. CO Adsorption and Oxidation. The dispersion of gold atoms into the oxide support in the form of substitutional point defects can lead to very active $Au_xCe_{1-x}O_2$ catalysts. The adsorption of a CO molecule with a surface O* atom neighboring the substitutional $Au^{\delta+}$ ion results in the direct CO oxidation without any activation energy. The interaction of a CO molecule placed at 2.0 Å from the surface O* apical atom of the octahedral Au ion leads to the spontaneous desorption of CO_2 via the formation of a surface O vacancy and the reduction of only one Ce ion (Figure 7a). The process releases −3.24 eV (GGA+U, Table 1). With respect to the stoichiometric $Au_xCe_{1-x}O_2$ surface, one excess electron resulting from the O vacancy formation occupies the gap state (B in Figure 6b) related to the Au−O* overlap, while the other occupies one Ce(f) state (D in Figure 7b), reducing the neighboring Ce ion to Ce^{3+}. On the basis of charge population analysis (Supporting Information) we interpret this substitutional Au ion as Au^{3+}.

After the release of the oxidation of a CO molecule, the substrate can promote a second oxidation when a CO molecule interacts with a surface O* atom of the planar AuO_4 moiety. The second oxidation has no activation barrier, is less exother-

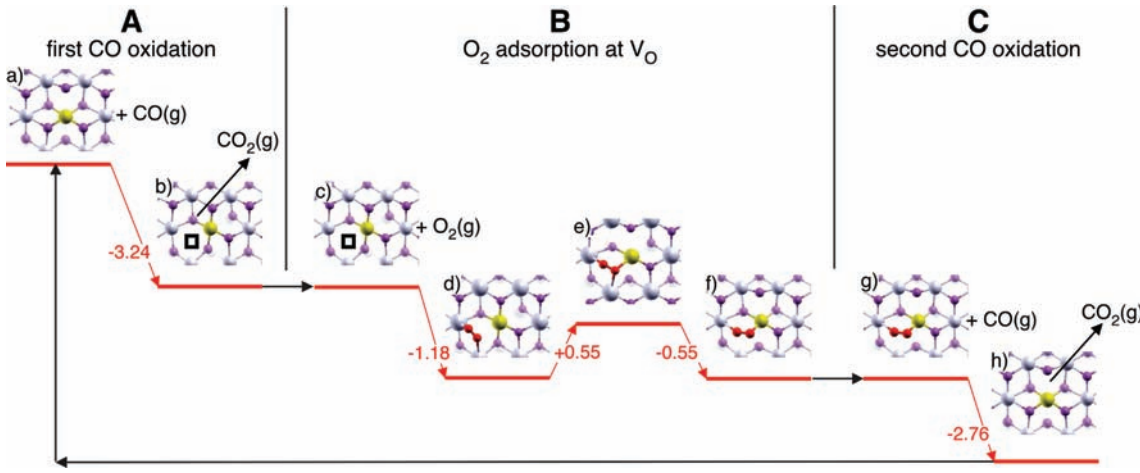

Figure 8. Calculated energetics for the CO oxidation promoted by a Au cation dispersed in a $Au_xCe_{1-x}O_2$ catalyst. The proposed catalytic cycle involves a first CO oxidation on the stoichiometric $Au_xCe_{1-x}O_2$ surface (A), with the adsorption of molecular O_2 (red circles) on the O vacancy (represented by a square) inducing a local rearrangement of the AuO_4 unit and the formation of O adspecies (B), and the reaction of a CO molecule with the O adspecies (C) recovering the stoichiometric $Au_xCe_{1-x}O_2$ catalyst.

mic (−2.34 eV, GGA+U value, Table 1) than the first one, and leads to the formation of a second O vacancy neighboring the Au ion (Figure 7b). In this case, the two excess electrons resulting from the formation of the second O vacancy do not the reduce further the ceria substrate, since only one Ce^{3+} is present in the cell before and after the second oxidation (state D and D_f in PDOS of Figure 7). Instead, one of these electrons occupies the Au(d) gap state C (see PDOS in Figure 7d) and the other the Au(s) state (labeled D_s in Figure 7d and displayed by gray areas), thus reducing the Au^{3+} ion to Au^+ (see charge analysis in the Supporting Information).

The difference between the reaction energies for the first and second CO oxidation reactions, −3.27 and −2.31 eV, respectively, is related to the different formation energy for creating one [0.32 eV, E_f^{Au/CeO_2} (I V_O) in Table 1] and a second [1.61 eV, E_f^{Au/CeO_2} (II V_O) in Table 1] oxygen vacancy close to a substitutional Au cation. The propensity of Au to form Au^{3+} ions together with the stability of the square-planar AuO_4 complex is on the basis of the small value for removing a surface O* from the stoichiometric $Au_xCe_{1-x}O_2$ surface. The formation of a second O vacancy close to the substitutional Au ion has a larger energy cost because of the electronic effects described above and because it breaks the square-planar AuO_4 complex: one O is removed, forming the vacancy, and the opposite O atoms with respect to the central Au ions relax away from Au by more than 1 Å, leading to a linear O−Au^+−O unit (Figure 7b) with Au−O bond lengths of 3.98 and 4.08 Å. The calculated energetics are reported in Table 1 and compared with the available literature.

These results are consistent with the general tendency of Au^{3+} to be readily reduced to Au^+ at room temperature, as observed in several spectroscopic measurements.[40] Moreover, we will show in the following that this catalyst can hardly be deactivated since the vacancies formed during the oxidation are ideal sites for dioxygen adsorption, leading to activated O adspecies[41] that can promote further CO oxidations.

4.2.2. Catalytic Cycle for CO Oxidation and Catalyst Regeneration. The structures and energetics discussed above for the oxidation of CO on $Au_xCe_{1-x}O_2$ surfaces suggest a catalytic cycle in which the positive oxidation state of the substitutional gold ion is preserved throughout the reaction and the catalyst is regenerated via vacancy filling by molecular O_2. This catalytic cycle, schematically represented in Figure 8, consists of three steps: (A) the oxidation of a first CO molecule on the stoichiometric $Au_xCe_{1-x}O_2$ surface through participation of a lattice oxygen, leading to O vacancy formation and CO_2 desorption (Figure 8 A); (B) The adsorption of molecular O_2 at the O vacancy, leading to the formation of surface adspecies (Figure 8 B); and (C) the interaction of a CO molecule with these O adspecies, which drives CO oxidation and regeneration of the stoichiometric $Au_xCe_{1-x}O_2$ surface (Figure 8 C).

The first step has been described in detail in the previous section and leads to the reduction of the substrate with one Ce^{3+} and one Au^{3+} close to the active sites (Figure 8a,b). The resulting surface O vacancy in front of the AuO_4 unit is then sealed by an oxygen molecule from the gas phase. The adsorption of the oxygen molecule on top of the O vacancy releases −1.18 eV and is accompanied by a relevant local rearrangement. Before O_2 adsorption (Figure 8c), the vacancy faces the AuO_4 unit in which the Au atom is coordinated by two O atoms of the first layer and by two O atoms of the second layer (at 2.14 Å). The calculated reaction path for O_2 adsorption (Figure 8d−f) reveals that the vacancy filling is a two-step process and involves two isoenergetic O_2−V_O binding configurations (Figure 8d,f). First the O_2 molecule finds a minimum (Figure 8d) at a height of 1.00 Å from the surface without binding directly to the Au ion (at 3.04 Å). In this configuration, the O−O bond length has already elongated from the gas-phase value of 1.21 to 1.32 Å, and the Ce^{3+} ion of the substrate reoxidizes to Ce^{4+}. An energy barrier of 0.55 eV separates this configuration from another one (Figure 8f) in which the molecule approaches further to the surface at a height of 0.59 Å. At the transition state of this reaction (Figure 8e), the Au ion breaks two Au−O bonds of the AuO_4 unit and binds to one oxygen atom of the O_2 adsorbate. This induces a rotation of the AuO_4 unit (see Figure 8f), which in the initial state was facing the vacancy, while in the final state it is transversal to the vacancy. This reorganization of the Au−O bonds is at the basis of the activation energy separating the two adsorption configurations. In this intermediate config-

(40) (a) Guzman, J.; Gates, B. C. *J. Phys. Chem. B* **2003**, *107*, 2242. (b) Minicò, S.; Scirè, S.; Crisafulli, C.; Visco, A. M.; Galvagno, S. *Catal. Lett.* **1997**, *47*, 273. (c) Guzman, J.; Gates, B. C. *J. Am. Chem. Soc.* **2004**, *126*, 2672.
(41) Huang, M.; Fabris, S. *Phys. Rev. B* **2007**, *75*, 81404(R).

uration (Figure 8f), the O−O distance is 1.33 and all the Au−O bond lengths of the rotated AuO_4 unit are between 1.09 and 1.15 Å.

The resulting O adspecies are activated by the presence of the neighboring Au ions and can promote the direct oxidation of a CO molecule, leading to the formation of CO_2, which desorbs without any activation barrier, releasing −2.76 eV (Figure 8g,h). The reaction was followed by placing a CO molecule at 1.9 Å from the surface O*−O* unit. This final step reoxidizes the catalyst, closes the cycle, and recovers the initial $Au_xCe_{1-x}O_2$ stoichiometric surface.

The three reaction steps are separated by the adsorption process of a molecule (CO or O_2) from the gas phase to the surface. In this way, the large exothermic nature of the catalytic cycle (more than 5 eV) is divided into smaller energy differences that are likely to be dissipated before the beginning of the following reaction step.

Since the $Au_xCe_{1-x}O_2$ surface can sustain multiple oxidation of CO, leading to the formation of two O vacancies close to the Au ion, we have also considered the possibility for a dissociative adsorption of molecular O_2 filling the two vacancies and recovering directly the stoichiometric surface. It turns out that the lowest energy path for this process involves first the adsorption of the molecule on one O vacancy (discussed above) and then the molecular dissociation followed by the diffusion of the O into the second vacancy. The rate-limiting step controlling this dissociative adsorption has a large activation energy, 1.70 eV, and is determined by the diffusion step, whose activation barrier is consistent with the calculated value for the diffusion of O adatoms on the stoichiometric (111) surface.[41] Given the large value of the energy barrier as compared to the steps B and C discussed above, we rule out the dissociative adsorption of O_2 on the divacancy formed by multiple oxidations on the $Au_xCe_{1-x}O_2$ catalyst.

Finally, we note that the same O adspecies are formed also when molecular O_2 adsorbs at the vacancies of the more reduced system (containing Au^+, Ce^{3+}, and two O vacancies as in Figure 7b) or even at isolated vacancies of the pure (111) CeO_2.[41]

4.2.3. Stability of the $Au_xCe_{1-x}O_2$ Catalyst during Reaction. A key intermediate state of the catalytic cycle identified above is the reduced surface resulting after the first CO oxidation (see Figure 8b,c). In this configuration, an O vacancy is formed nearby the Au ion that occupies a Ce lattice site. Ab initio thermodynamics studies predict Au adsorption into the O vacancy to be strongly preferred to that into the Ce vacancy.[17b] It is therefore important to assess the stability of the intermediate state toward the diffusion of the Au ion from the Ce vacancy into the O vacancy. This event would then yield the deactivation of the $Au_xCe_{1-x}O_2$ system, similarly to the case of the Au adatom supported by the stoichiometric surface.

In order to verify the stability of this intermediate step, we have displaced the Au atom from the Ce vacancy into the O vacancy, as shown in Figure 9a, and allowed the system to relax according to the Hellman−Feynman forces. The evolution of the total energy during the relaxation is displayed in Figure 9 and shows that the position of the Au atom into the O vacancy is unstable in the presence of a neighboring Ce vacancy. The Au adatom is strongly attracted toward the neighboring Ce vacancy and spontaneously reaches a metastable configuration (Figure 9b) that is several electronvolts lower in energy than the initial structure (Au on top of the O vacancy). With respect to this configuration, the energy is further lowered by 0.62 eV when the Au atom occupies the Ce site (Figure 9c), thus proving

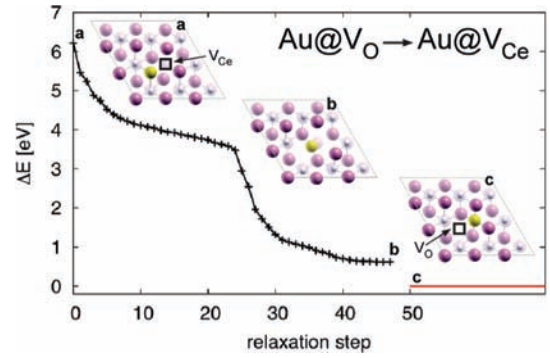

Figure 9. Stability of the intermediate state of the catalytic cycle shown in Figure 8b,c. Energy evolution during the structural relaxation of a Au adatom initially on top of an O vacancy close to a Ce vacancy (a). The Au adatom is attracted into the Ce vacancy and reaches a metastable configuration (b), which is 0.62 eV higher in energy than the most stable structure where the adatom substitutes for the Ce vacancy in the presence of a neighboring O vacancy (c). Energies are relative to the total energy of the latter structure.

that the intermediate structure of the catalytic cycle (Figure 8b,c) is stable toward the diffusion of the substitutional Au atom from the Ce vacancy to the surface O vacancy site.

Conclusions

In conclusion, we provide insight into the catalytic mechanisms by which single gold atoms promote the oxidation of CO on CeO_2(111) surfaces. The calculations predict the selective absorption of molecular CO on small Au clusters and support the correlation between the presence of positively charged Au atoms and the reactivity toward CO oxidation. Isolated adatoms supported by stoichiometric ceria (111) surfaces are shown to induce charge redistribution at the metal/oxide contact, leading to the reduction of the ceria substrate and resulting in lattice Ce^{3+} and surface Au^+ ions. The oxidation reaction is controlled by the molecular spillover from the Au^+ adatom to the oxide support, forming a metastable Au−COO* configuration (MS in Figure 5) in which the CO molecule bridges between the Au^+ and the closest lattice O* atom. The calculated activation barrier for this process is 0.86 eV. Oxidation and CO_2 desorption takes advantage of the oxygen buffering capacity of ceria and leads to the formation of a surface O vacancy with an activation energy of only 0.24 eV. However, during this reaction, the Au^+ adatom diffuses into the vacancy and turns into negatively charged $Au^{\delta-}$ adspecies that prevents the adsorption of molecular CO or O_2, thus deactivating the catalyst. It is suggested that this last step can be hindered by the Au−Au cohesive energy in supported clusters of larger size. While the $Au^{\delta-}$ species on O vacancies are inactive for CO oxidation, they strongly favor the aggregation of further Au adatoms. We provide evidence that the activity toward CO oxidation by Au nanoparticles nucleated at O vacancies can be recovered for cluster sizes as small as Au_2.

Quite differently, $Au_xCe_{1-x}O_2$ solid solutions in which Au substitutes for Ce lattice sites are more active than single Au^+ species supported on the stoichiometric oxide surface, although the stability of these structures is still an open issue. These systems can sustain a catalytic cycle in which the oxidation state of the dispersed Au ions remains positive and can promote multiple CO oxidations without any activation energy. The oxidation results in the formation of surface O vacancies and is assisted by reversible Au^{3+}/Au^+ and Ce^{4+}/Ce^{3+} reductions. Molecular oxygen can seals these vacancies, forming activated

O adspecies and leading to a local rearrangement of the AuO_4 unit activated by an energy barrier of 0.55 eV. Molecular CO is then shown to react with these O adspecies without activation energy, forming CO_2 and recovering the initial stoichiometry of the $Au_xCe_{1-x}O_2$ system. These results rationalize recent experimental evidence on the activity of positively charged Au atoms toward oxidation reactions and are the starting point for the study of the catalytic properties of larger Au clusters supported on reducible oxides.

Acknowledgment. We are grateful to Stefano Baroni for fruitful discussions. We acknowledge the INFM-CNR and CINECA "Progetto Calcolo Parallelo" for computer resources.

Supporting Information Available: Charge population analysis and molecular modeling coordinates. This material is available free of charge via the Internet at http://pubs.acs.org/.

JA902109K